A DOUBLE-CORNER SOURCE SPECTRUM FOR 5.3 ≤ M ≤ 7.7 THAT PREDICTS PGA, PGV, DURATION, RADIATED ENERGY AND APPARENT STRESS

C. JI[1,2] AND R. J. ARCHULETA[1,2]

[1]Department of Earth Science, University of California, Santa Barbara, USA
[2]Earth Research Institute, University of California, Santa Barbara, USA

E-mail contact of main author: ji@geol.ucsb.edu

Abstract. We show that a double-corner source spectrum can reproduce the peak ground acceleration (PGA) and peak ground velocity (PGV) of the NGA West-2 data set for magnitudes 3.3 to 7.7. The two corners scale with magnitude; however, the scaling is different for magnitudes above and below 5.3. A double-corner spectrum can explain why the average stress drop from seismological studies is different from the stress parameter used to estimate PGA and PGV. Here we focus our analysis and conclusions for M ≥ 5.3. The two corners f_{c1} and f_{c2} scale as $\log(f_{c1}(M)) = 1.754 - 0.5M$ and $\log(f_{c2}(M)) = 3.250 - 0.5M$. Both are proportional to $0.5M$ indicating self-similar scaling with magnitude. The lower corner f_{c1} is within 18% of the corner one would observe from the global CMT catalog, i.e., it's inverse $1/\pi f_{c1}$ corresponds to the duration of earthquakes found worldwide. The acceleration spectrum is proportional to f^1 between f_{c1} and f_{c2}. The acceleration spectral level at frequencies greater than f_{c2} is consistent with PGA and PGV for earthquakes in the NGA West-2 data. This high-frequency spectral level is proportional to the stress parameter used in time domain stochastic predictions of PGA and PGV. The radiated energy and the apparent stress agree with global estimates of these parameters for the same magnitude range.

Key Words: Magnitude scaling, source spectrum, double corner, PGA and PGV

1. Introduction

Gusev [*1*] provides an excellent summary of papers ([*2*], [*3*], [*4*], [*5*], 6], [*7*], [*8*]) that produce a double-corner Fourier amplitude acceleration spectrum which has a basic shape $f^2 - f^1 - f^0$ as frequency increases from its lowest to highest values. The spectrum has two corner frequencies f_{c1} and f_{c2} where $f_{c2} > f_{c1}$. Brune [*3*] showed that such a spectrum could arise from a partial stress drop, namely, a static stress drop that is less than the dynamic stress drop. Models [*4*], [*6*], [*7*] share a common property of having a subevent embedded in a larger slip area. The lower corner f_{c1} is related to the overall duration for faulting while the higher corner f_{c2} is related to the duration of faulting of the subevent. Similarly, Heaton's [*8*] propagating slip pulse has the overall duration of faulting and a duration related to the slip pulse. A propagating slip pulse is analogous to a propagating partial stress drop. In all of these models there is an explicit assumption that the subevent (asperity/barrier) has a higher stress drop compared with the average stress drop of overall faulting.

Aki [*9*] illustrated that 14 earthquakes, all with M ≥ 6.0, produced strong motion was consistent with local stress drop on the order of 20-40 MPa, compared with the global average of 3-4 MPa [*10, 11*]. Earlier papers [*12*], [*13*] had reached a similar conclusion; both papers deduced a subevent(s) with stress drops much larger than the average stress drop. Analyzing data from earthquakes in Italy and Montenegro, Faccioli [*14*] concluded that the observed high-frequency radiation in accelerograms "is dominated by the radiation from one, or a few compact subsources." Faccioli [*14*] generalized the double-corner spectrum implied by Haskell's [*15*] model to incorporate a subevent and a main event. Faccioli [*14*] proposed that the stress drop of the subevent would scale as $M_0^{1/4}$ where M_0 is seismic moment. Atkinson [*16*] developed

an additive model for the acceleration spectrum in order to explain double corner acceleration spectra observed in the eastern North America where the first corner scaled by about $M_0^{-1/3}$, i.e., nearly self-similar scaling [*17*]. Garcia et al. [*18*] explained the acceleration spectra of intraslab earthquakes in the Mexican subduction zone with a double corner—one related to the overall source dimension and another to the subevent. Their scaling of the first corner is approximately self-similar; the second corner scaling is not self-similar.

Atkinson and Hanks [*19*] proposed a high-frequency magnitude scale to reflect the spectral level at high frequencies. The average stress drop from the high frequency spectral level were 8.3 and 14.7 MPa, for 28 California and 28 North Eastern America earthquakes, respectively. Atkinson and Beresnev [*20*] succinctly framed the entire concept by referring to a stress parameter as the controlling agent of the high frequency spectral level. Boore et al. [*21*] examined both a multiplicative and additive functional form for a double corner spectrum. The low-frequency level is controlled by seismic moment and the high-frequency level is controlled by the stress parameter. They showed that they could satisfy the SCEC broadband tests [*22*] for predicting response spectra using the additive form in stochastic simulations using SMSIM [*23*].

Baltay and Hanks [*24*] employed a classic stochastic approach [*25*] to explain the observed root-mean-square (a_{rms}) and peak ground accelerations (PGA) in the NGA West-2 data [*26*]. This was extended to predict the peak ground velocities (PGV), Wood-Anderson seismograph response and response spectra [*27*]. The method was improved by including path attenuation and site effects [*28*], [*29*], [*30*]. Baltay and Hanks [*24*] found that the scaling relations of mean PGAs and PGVs with magnitudes from 3 to 8 can be simultaneously modeled fairly well using a point-source Brune model [*3*] with a constant stress drop of 4.64 MPa and the high-frequency attenuation parameter κ_0 [*28*] of 0.04 s, random vibration theory, and a finite-fault assumption at the large magnitudes.

As pointed out earlier [*20*], the Brune type stress drop ($\Delta\sigma_B$) in stochastic modeling is not necessarily equal to the average static stress drop of the target earthquake and may be better to be viewed as a "parameter" that controls the high frequency level. For Brune's spectrum with a corner frequency f_c, the high frequency acceleration spectrum level scales as $M_0 f_c^2$, with $f_c = 0.49\beta(\frac{\Delta\sigma_B}{M_0})^{1/3}$. The magnitude independent $\Delta\sigma_B$= 4.64 MPa found to fit PGA and PGV [*24*] is equivalent to the scaling relation $\log(f_c^s) = 2.441 - 0.5\,M$, M is moment magnitude; f_c^s is S-wave corner frequency. (Throughout this paper we use moment magnitude [*31*], though it will not be shown as bold case M.) For comparison, Allmann and Shearer [*11*] conducted a global survey for the stress drop of M>5 earthquakes using the P-wave corner frequency (f_c^P) of observed P wave spectra and Madariaga's relation, $\Delta\sigma_M = \frac{7}{16}M_0(f_c^P/0.32\beta)^3$ [*32*]. For the events with at least 20 records they found that an average stress drop of 3.36 MPa. While this value is very close to the average stress drop of 3 MPa [*10*], it is also model dependent. By assuming a f_c^p/f_c^s ratio of 1.6 [see review in *30*], Allmann and Shearer's [*11*] result is equivalent to $\log(f_c^s) = 2.164 - 0.5\,M$. The difference of 0.277 in the constant (2.441 vs. 2.164) between these two scaling relationships suggests that the corner frequency needed to fit the PGA and PGV in the NGA-West 2 dataset [*24*] is 1.89 times larger than the average S-wave corner frequency of global earthquakes with the same magnitude. With stress drop proportional to f_c^3, the stress drop used to model the high frequency radiation that determines PGA and PGV is 6.8 times of the average stress drop of global earthquakes. It is 22.8 MPa in

$\Delta\sigma_M$. Hence, the earthquake source spectrum seems to have two critical frequencies: one is related with the average property of source rupture and a second associated with high frequency radiation. Both apparently scale with magnitude with a slope of 0.5, i.e., self-similarity.

Archuleta and Ji [*33*] noticed the nearly pure linear relations of mean LogPGA, LogPGV and "dominant frequency" (DomF= $\frac{1}{2\pi}\frac{PGA}{PGV}$) with magnitude M, 3.3 <M<5.3, in NGA-West2 dataset, The model of Baltay and Hank's [*24*] does not explain PGA and PGV in this magnitude range as well as it does for higher magnitudes. Archuleta and Ji [*33*] proposed a magnitude dependent apparent moment rate function (aMRF) in the time domain:

$$\dot{M}_0(t) = \begin{cases} at^2 & for\ t \in [0, \tau_p] \\ a{\tau_p}^2 \frac{(\tau_d - t)}{\tau_d - \tau_p} & for\ t \in [\tau_p, \tau_d] \end{cases} with\ a = M_0 / [\tfrac{1}{2}{\tau_p}^2 \left(\tau_d - \tfrac{1}{3}\tau_p\right)] \qquad (1)$$

The peak time τ_p and the duration τ_d have following scaling relationships with seismic moment M_0,

$$\tau_d(M_0) = {\tau_d}^{ref} \left({M_0}/{M_0^{[ref]}} \right)^{1/3+\epsilon_d} \ \&\ \tau_p(M_0) = {\tau_p}^{ref} \left({M_0}/{M_0^{[ref]}} \right)^{1/3+\epsilon_p} \qquad (2)$$

Here, ${\tau_d}^{ref}$, ${\tau_p}^{ref}$ are peak time and duration of the reference event with seismic moment M_0^{ref}. In Archuleta and Ji [*33*], the selected reference event has a magnitude of 3.3. Its peak time and total duration are $\tau_p^{[3.3]}$ and $\tau_d^{[3.3]}$. A grid search procedure is adopted to find the optimal values of the five parameters (t*, ${\tau_d}^{[3.3]}$, ${\tau_p}^{[3.3]}$, ϵ_d, ϵ_p) that satisfy the scaling relations between seismic moment and LogPGA, LogPGV, DomF as well as the logarithm of peak Wood-Anderson amplitude (LogPWA) simultaneously. They tested more than 18 million combinations [*33*]. Two optimal solutions are summarized in Table 1. Because of the strong trade-off between t* and $\tau_p^{[3.3]}$, the inverted result is not unique. Model I is the model with the smallest misfit, but it is associated with a large t* of 0.066s. Model II is the best model with a more reasonable t* of 0.054 s. It should be noted that even though there is a factor of three

Table 1. *Model Parameters*

Models	t^*	$\tau_p^{[3.3]}$	ϵ_p	$\tau_d^{[3.3]}$	ϵ_d	*error*	$\tau_p^{[5.3]}$	$\tau_d^{[5.3]}$
Model I [33]	*0.066 s*	*0.01 s (ref)*	*0.1*	*0.31 s (ref)*	*0.5*	*0.167*	*0.093 s (pred.)*	*2.23 s (pred.)*
Model II [33]	*0.054 s*	*0.03 s (ref)*	*4.0*	*0.31 s (ref)*	*0.3*	*0.520*	*0.080 s (pred.)*	*2.51 s (pred.)*
Model N (this study)	*0.054 s*	*0.008 s (pred.)*	*0.0*	*0.25 s (pred.)*	*0.0*	*NaN*	*0.080 s (ref)*	*2.51s (ref)*

$\tau_p^{[3.3]}$ and $\tau_p^{[5.3]}$ are peak times for M 3.3 and M 5.3 respectively.

difference in $\tau_p^{[3.3]}$ between these two models, the difference in $\tau_p^{[5.3]}$ is only 15%. The trade-off between t* and τ_p becomes less significant for moderate-sized earthquakes.

Figure 1a shows a normalized aMRF using τ_p and τ_d time for a M 5.3 earthquake. Note that the seismic moment rate increases sharply to the peak in 0.08 s (or 0.25 s after considering the

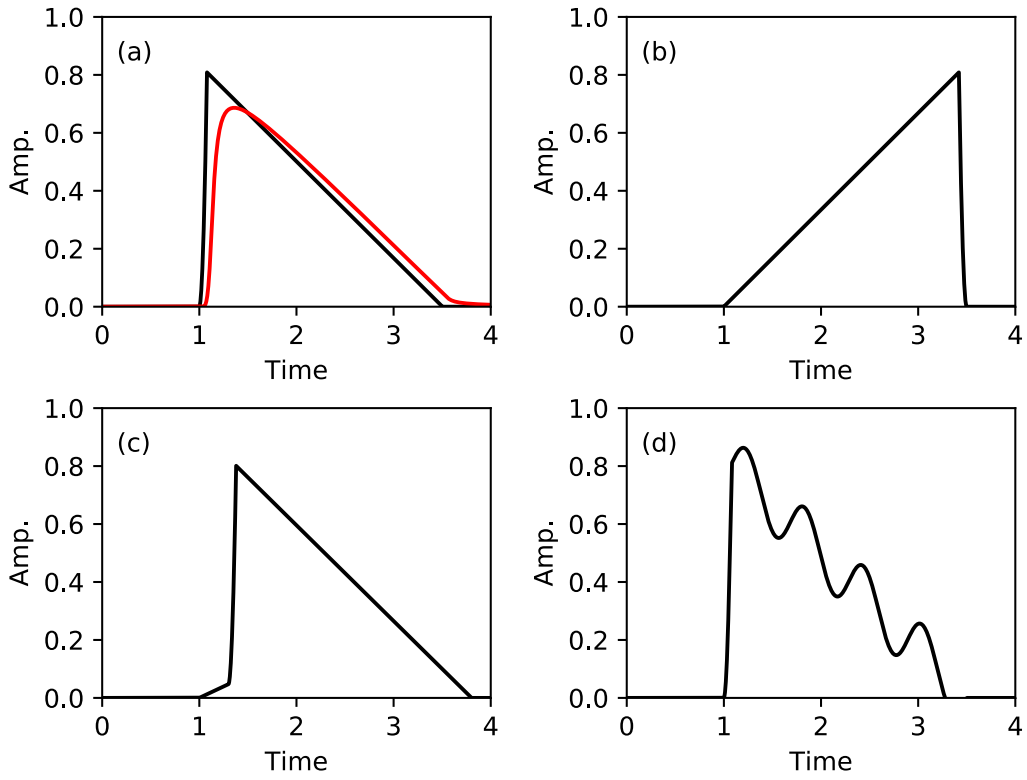

FIG. 1. Comparison of four apparent moment rate functions that satisfy the observations (a) Normalized apparent moment rate function (black line) defined by equation (1) with τ_p=0.08 s and τ_d =2.5 s. The red line denotes the aMRF after considering the distortion caused by earth attenuation with a t=0.054 s. (b) temporal "mirror" of the function in (a). (c) function in (a) with additional small "nucleation" phase. (d) function in (a) with additional oscillation between τ_p and τ_d.*

attenuation). Although Meier et al. [*34*] recently reported that most earthquakes initiated sharply in first 0.1 s, consistent with this model, one is cautioned to remember that the proposed aMRF can only be viewed as a representative MRF; an aMRF is dependent on the azimuth due to directivity. Because there is no temporal information in the datasets of PWA, PGV, PGV, and DomF, the solution is not unique. For instance, the temporal "mirror" of the proposed aMRF (Figure 1b) or the addition of a small "nucleation" phase [*35*] at the beginning (Figure 1c) will fit the data equally well. It is important to recognize that the temporal variation between τ_p and τ_d has few constraints. The moment rate variation during this period is almost certain to be more complicated than the linear decrease. Such intrinsic non-uniqueness in phase information leads us to investigate the source amplitude spectrum and explore whether it is possible to explain the entire magnitude range using random vibration theory.

1. A magnitude dependent double-corner source spectrum

Archuleta and Ji [*33*] noticed that when $\tau_p \ll \tau_d$, the spectrum of the proposed aMRF satisfies,

$$|\dot{M}_0(f)| \propto \begin{cases} 1 & f < f_{c1} \\ 1/f & f_{c1} < f < f_{c2} \\ 1/f^2 & f > f_{c2} \end{cases} \quad (3)$$

with corner frequency $f_{c1} = 1/(\pi\tau_d)$ and $f_{c2} = 1/(\pi\tau_p)$. A more general form of the double-corner spectrum that satisfies equation (3) might be represented as

$$\Omega(f, M_0, \gamma, f_{c1}, f_{c2}) = \frac{M_0}{\left[1+(\frac{f}{f_{c1}})^{\gamma}\right]^{1/\gamma}\left[1+(\frac{f}{f_{c2}})^{\gamma}\right]^{1/\gamma}} \quad (4)$$

γ might be called Boatwright parameter [*36*]. Note that when γ=2 and f_{c1}=f_{c2}=f_c, the function becomes Boatwright ω^{-2} displacement spectrum [*36*]. Boore [*23*] summarized several models that had a double-corner, including Haddon [*37*], though Haddon did not publish that form in his paper. According to [*23*], Haddon [*37*] adopted equation (4) with γ=8 as his source model. The scaling relations for corner frequency he proposed are $\log(f_{c1}) = 2.3 - 0.5\mathrm{M}$ and $\log(f_{c2}) = 3.4 - 0.5\mathrm{M}$. Compared to equation (10) there is a 0.55 difference in the constant for $\log(f_{c1})$. Coincidentally, it is close to the value of $\log(\pi)$ (~0.5); there is a difference of 0.15 for $\log(f_{c2})$.

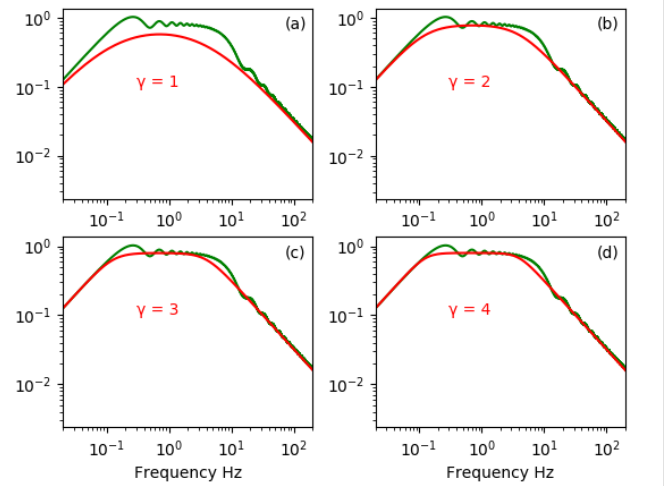

FIG. 2. Comparison of the velocity spectra of two normalized aMRF functions ($M_0 = 1$). The green curve denotes the velocity response of A&J aMRF [33] function with τ_p=0.08 s and τ_d=2.5 s. The red curve denotes the velocity response of equation (4) with $f_{c1} = 1/(\pi\tau_p)$ and $f_{c2} = 1/(\pi\tau_d)$. The parameter γ is equal to 1, 2, 3, 4 for (a), (b), (c) and (d), respectively.

The shape of the velocity spectrum for $|2\pi f\dot{M}_0(f, \tau_p, \tau_d)|$ and $|2\pi f \cdot \Omega(f, M_0, \gamma, f_{c1}, f_{c2})|$ are compared in Figure 2. The parameters used are: $\tau_p = 0.08$ s, $\tau_d = 2.5$ s, $f_{c1} = 1/(\pi\tau_p)$, $f_{c2} = 1/(\pi\tau_d)$, and $M_0 = 1$. As we expect, $|2\pi f\dot{M}_0(f)|$ has the flat "plateau" shape as expected though it is accompanied by oscillations with decaying amplitude near its two corners. The shape of $|2\pi f \cdot \Omega(f)|$ depends on the value of γ. In fact, when $\gamma = 1$, it is difficult to visibly judge whether it has two corner frequencies. When γ is greater, the corners of the spectrum become sharper. The discrepancy between the two spectra becomes smaller when γ increases. With no significant change for $\gamma > 3$, we use γ=4 in our modeling.

Our goal is to explain the PWA, PGV, PGA, DomF relationships using double-corner source spectrum in equation (4). The scaling relationships of τ_p and τ_d in equation (2) can be replaced with the following scaling relationships of f_{c1} and f_{c2} with moment magnitude M,

$$\log\left(f_{c1}(M)\right) = \log\left({f_{c1}}^{ref}\right) - \frac{1.5}{3+\epsilon_d}(M - M^{ref}) \quad (5a)$$

$$\log\left(f_{c2}(M)\right) = \log\left({f_{c2}}^{ref}\right) - \frac{1.5}{3+\epsilon_p}(M - M^{ref}) \quad (5b)$$

Here, ${f_{c1}}^{ref}$, ${f_{c2}}^{ref}$ are the corner frequency of the M^{ref} reference event. Thus ${f_{c1}}^{ref}$, ${f_{c2}}^{ref}$, ϵ_d and ϵ_p are four input parameters for this source models.

2. Forward modeling

In a half-space, the amplitude spectra of observed P or S wave displacement, velocity and acceleration can be represented as

$$\tilde{D}(f) = CM_0\,\Omega(f)e^{-\pi f t^*} \quad (6a)$$

$$\tilde{V}(f) = CM_0\,\Omega(f)e^{-\pi f t^*}2\pi f \quad (6b)$$

$$\tilde{A}(f) = CM_0\Omega(f)e^{-\pi f t^*}4\pi^2 f^2 \quad (6c)$$

$C = \frac{\sqrt{2}R_{\theta\varphi}Amp}{4\pi\rho\beta^3 R}$ denotes the combination effect of source radiation pattern, wave propagation, near-surface and site effects [e.g., *27*]. Our modeling is for the S wave. $R_{\theta\varphi}$ is average radiation factor—0.63 for an S wave; β is the S wave velocity at the source region; R denotes the shortest distance to the rupture plane; Amp represents the site effect; t^* denotes the effect of earth attenuation. Ω(f) is the Fourier transform of the aMRF(t). We will use equation 4 as our spectral shape. The Wood Anderson spectrum is $\widetilde{D_{WA}}(f) = |I_{WA}(f)|\,\tilde{D}(f)$ where $I_{WA}(f)$ is the Wood Anderson instrument response.

Using the Parseval's Theorem, the root-mean-square Wood Anderson displacement (WA_{rms}), root-mean-square velocity (V_{rms}) and root-mean-square acceleration (a_{rms}) can be related with the source amplitude spectra,

$$WA_{rms} = \sqrt{\frac{2\int_0^\infty [\widetilde{D_{WA}}(f)]^2 df}{T}} \quad (7a)$$

$$V_{rms} = \sqrt{\frac{2\int_0^\infty [\tilde{V}(f)]^2 df}{T}} \quad (7b)$$

$$a_{rms} = \sqrt{\frac{2\int_0^\infty [\tilde{A}(f)]^2 df}{T}} \quad (7c)$$

T denotes the duration of aMRF. By assuming the phase of velocity and acceleration time history is random V_{rms} and a_{rms} are linked with PGV and PGA [*38*], [*23*] using random vibration theory [*39*],

$$\frac{Peak}{rms} \approx \sqrt{2\ln(N)} + \left(\frac{\gamma}{\sqrt{2\ln(N)}}\right) \quad (8)$$

γ =0.5772… is Euler's constant. N is number of zero crossings in the corresponding time histories over a source duration $T = 1/(\pi f_{c1})$. Although most previous studies used Brune's [*3*] source spectrum to explain the scaling relationships of strong motion parameters, [*27*] and [*29*] paved the way to directly estimate them. For example, using N_a to denote the N in the acceleration time history, it can be estimated with the relation,

$$N_a = \frac{T}{\pi}\int_0^\infty \left[\tilde{A}(f)2\pi f\right]^2 df \Big/ \int_0^\infty \left[\tilde{A}(f)\right]^2 df \quad (9)$$

Note that equation (8) is a good approximation only when N_a is large. Following [*29*], we ask for N>2. Because the signals progressively contain more high frequency energy going from Wood Anderson displacement to velocity to acceleration, N estimated by equation (9) has to increase as well. As mentioned above, equation (8) is a good approximation only when N is large, for example N>2. For the smallest magnitude that we investigate, M=3.3, N is 1.6 for Wood Anderson displacement waveforms, 2.5 for velocity waveforms, and 5.1 for acceleration waveforms, increasing progressively over a duration of 0.25 s. Thus, for PWA, we only look at the estimates for M>3.7 events.

Following our previous analysis [*33*], we assume Amp=2.4 and t^*=0.054 s, though each are case dependent [e.g., *27*] and deserve more consideration in a future effort. We adopt 3.5 km/s as the S-wave speed in the source region. In the following forward simulation, we use M^{ref}=5.3. Because Model II is associated with a more reasonable t^* of 0.054 s, $\tau_p^{[5.3]} = 0.08\ s$ and $\tau_d^{[5.3]} = 2.5\ s$ are chosen. With equations (5a, 5b) the corresponding ${f_{c1}}^{ref}$ and ${f_{c2}}^{ref}$ are 0.127 Hz and 3.980 Hz, respectively. We assume a self-similar source model for M > 5.3, i.e., both ϵ_d and ϵ_p are equal to zero in equation (5a, 5b). With these conditions the two corner frequencies satisfy:

$$\log\left(f_{c1}(M)\right) = 1.754 - 0.5M$$
$$\log\left(f_{c2}(M)\right) = 3.250 - 0.5M \quad (10)$$

With these values, we can computer the root-mean-square values for PGA, PGV and PWA, from which we can compute the peak values assuming random vibration theory.

Figure 3a shows the predicted peak Wood Anderson displacement (PWA). In practice, PWA is defined as half of maximum peak-to-peak amplitude. When moment magnitude M increases two units from 3.7 to 5.7, the PWA amplitude increases 56 times, suggesting a M_L increases of 1.75, just slightly smaller. But when M increases from 5.7 to 7.7, the PWA amplitude increases only 15 times, an increase of only 1.2 units in M_L. Overall the model explains the data—PGV, PGA, DomF as a function of magnitude—fairly well (Figure 3 b, c and d, respectively). However, the model cannot produce the sharp change in slope near M 5.1.

For M 5, 6 and 7 we compare (Figure 4) our spectrum with the double-corner spectrum from Atkinson and Boore [*40*], the single-corner spectrum from Baltay and Hanks [*24*], and the single-corner spectrum from Allmann and Shearer [*11*].

The parameters for the double corner in [*40*] are based on earthquakes in eastern North America. In computing the coefficient C (equation 6) we have used 3500 m/s for the S-wave velocity and 2700 kg/m^3 for density for all of the relations. In this way the low-frequency limit is identical for each relation.

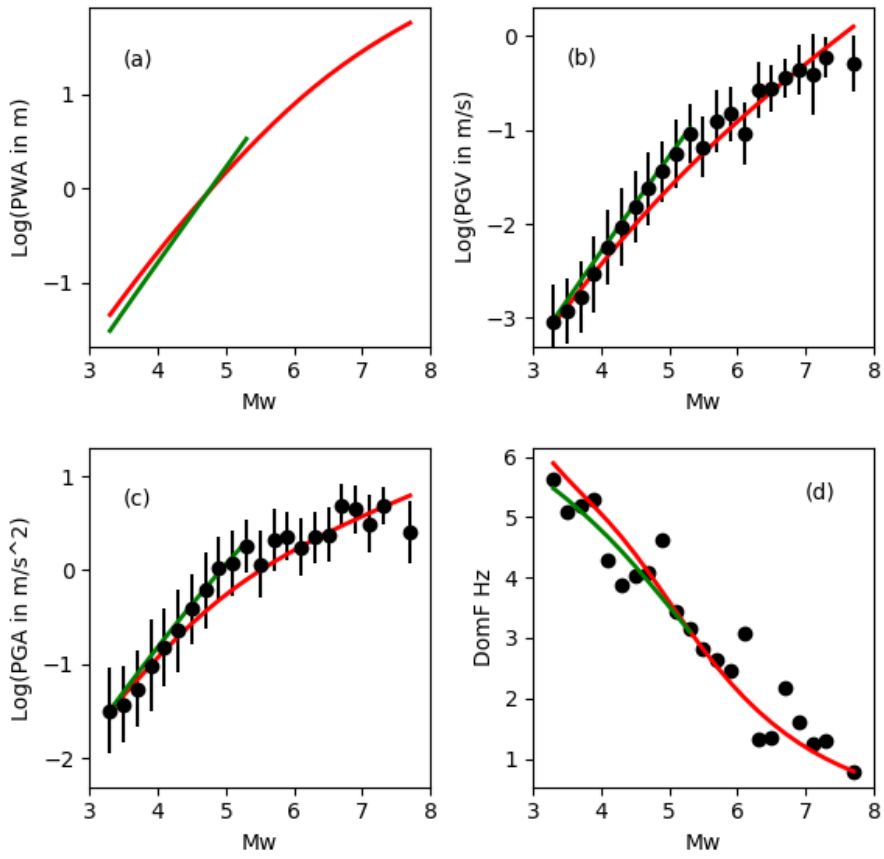

FIG. 3. Comparison of data (black dots) and synthetic predictions PWA, PGV, PGA, and DomF (red curves) in a, b, c and d, respectively. The synthetics for 3.3≤M≤5.3 using time domain method (2) are shown as green lines. Note that the maximum discrepancy in |log(Obs/syn)| is 0.36, which is compatible with 1σ standard deviation (0.32-0.35 for M 5.1)

As mentioned above, the corner frequency is derived from their magnitude independent stress drop of 4.64 MPa [*24*]. Allmann and Shearer [*11*] found a global average stress drop of 3.36 MPa (with $f_c^p / f_c^s = 1.6$ [*32*]). Note that our double-corner spectrum does not depend on any assumption of a stress drop. It is based on having two, time durations and assuming self-similar scaling, $Logf_x \sim 0.5M$. The double corner spectrum does fit the PGA and PGV of NGA West-2; hence its level at high frequencies is comparable to [*24*] who inverted for a stress drop consistent with PGA and PGV in NGA West-2. Baltay and Hanks [*24*] constrained their model to be single corner spectrum that matched the seismic moment and the high-frequency spectral level. Their corner frequency is about a factor of two larger than that found by Allmann and Shearer [*11*] who inverted teleseismic observations to find a corner frequency. Allmann and Shearer [*11*] used Madariaga's [*41*] model to compute a stress drop. Their single time duration (single corner) is the overall duration of the earthquake. As one can see, this model will under-predict PGA and PGV by about a factor of 7. However, its corner is consistent with the duration of earthquakes M ≥ 5.5, while Baltay and Hanks [*24*] duration is shorter by almost a factor of 1.9.

3. Discussions

3.1 Scaling law for earthquake total duration

At a first glance, it appears that we need one more parameter than Baltay and Hanks [*24*] to model the same dataset. However, we find that the scaling relation of f_{c1} agrees with the long period property of earthquake source that has been long recognized. In the routine process of

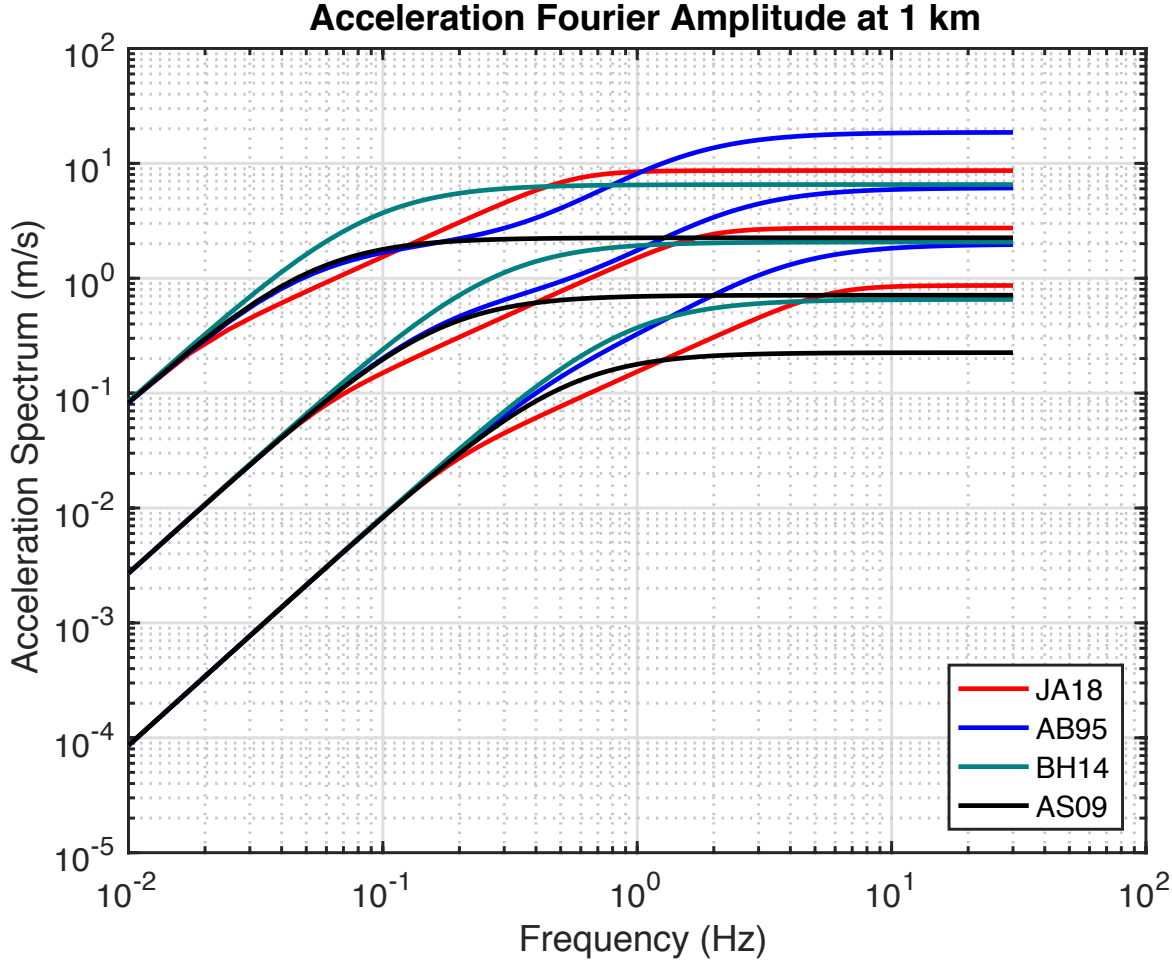

FIG. 4. Acceleration Fourier amplitude spectrum from four models: JA18, this paper with the two corners given in equation (10); AB95, (40) with two corners and a variable epsilon dependent on magnitude; BH14, (24) and AS09, (11). BH14 and AS09 are single corner spectra; AB95 and JA18 are double-corner spectra. JA18 always has a f^1 form between the two corners; AB95 has a shape that depends on a variable epsilon that is magnitude dependent. AS09 has a corner frequency determined from a global average stress drop (3.36 MPa) independent of magnitude; the corner frequency in BH14 comes from a magnitude-independent stress drop (4.64 MPa) that was the best inverted solution, including a site attenuation of 0.04 s, to fit PGA and PGV in the NGA West-2 database for $3.0 \leq M \leq 8.0$.

Global CMT project (http://www.globalcmt.org), the source time function is assumed to be a boxcar with a half duration T_h that is scaled with seismic moment, $T_h = 2.26 \times 10^{-6} {M_0}^{1/3}$ [*42*]. This relation was inferred from previous body wave analysis of teleseismic events [e.g., *43*]. The width of the boxcar ($2T_h$) is a good prediction to the "effective" source duration, i.e., the smallest rupture time over which 95% of the total moment is released [*44*]. A boxcar function has a f^{-1} source spectrum with corner frequency $1/(\pi T_{GCMT})$, T_{GCMT}=$2T_h$. The inferred scaling relationship is

$$\log\left(f_c^{GCMT}(M)\right) = 1.831 - 0.5M \qquad (11)$$

or equivalently $\log\left(T_{GCMT}(M)\right) = 0.5M - 2.33$. Combining equations (10) and (11), we have $f_c^{GCMT} \sim 1.19\, f_{c1}$. This is within the uncertainty of T_h and $\tau_d^{[5.3]}$ (Reference duration, see Table

1). We tested the use of equation (11) to define f_{c1} and found that it produces equal or better fits for the magnitude range from 4.5 to 7.3 than equation (10) but slightly worse fits for smaller magnitude events.

Alternatively, we also can compare the inferred source duration ($\tau_d(M)$) from our model, which satisfies $\log(\tau_d(M)) = 0.5M - 2.25$, with the expected source duration inferred from the corner frequency of ω^{-2} source spectra, $\log(f_c^s) = 2.164 - 0.5\,M$ [*11*]. They used an empirically based f_c^p/f_c^s ratio of 1.6. Though it is often assumed that rupture duration is closely allied with $1/f_c$ in the ω^{-2} source model, e.g. [*27*], an additional assumption about the shape of apparent moment rate function needs to be made because we only have amplitude information. If we assume that the apparent moment rate function has a symmetric shape, the predicted source duration will be shorter. The simplest symmetric time domain function that satisfies the ω^{-2} source spectrum is probably the isosceles triangle function. Its corner frequency and duration T have the relation $f_c = 2/\pi T$. The predicted source duration scaling relation is $\log(T_T(M)) = 0.5M - 2.36$, where T_T denotes the isosceles triangular source time function. $T_T(M)$ is 9% smaller than $T_{GCMT}(M)$ and 22% smaller than $\tau_d(M)$ defined above. Kanamori and Rivera [*44*] proposed another symmetric time function that satisfies the ω^2 model, $\Omega(t) = \frac{6M_0}{T^3}t(T-t)$, $t \in [0,T]$. Its corner frequency and source duration follow the relation $f_c = \sqrt{12}/2\pi T$ [*30*]. The predicted source duration T_{KR} satisfies, $\log(T_{KR}(M)) = 0.5M - 2.42$. It is 19% smaller than $T_{GCMT}(M)$, and 32% smaller than $\tau_d(M)$. In contrast, Brune [*3*] proposed an asymmetric source time function that satisfies ω^2 spectra, $\Omega_B(t) = M_0(2\pi f_c)^2 t e^{-2\pi f_c t}$, which has been widely used in the community. This function has an infinitely long tail, but the "effective" source duration mentioned above satisfies, $\log(T_B(M)) = 0.5M - 2.27$, falling in between $T_{GCMT}(M)$ and $T(M)$.

In summary, the scaling relations of total duration $\tau_d(M)$ or corner frequency f_{c1}, inferred from the analyses of the close-fault strong motion dataset, NGA-West2, agree with previous seismological results based on distant broadband or long period information remarkably well.

3.2 Earthquake energy budget

For an earthquake with ω^2 source spectrum, PGA scales with the corner frequency as $f_c^{2.5}$ [*45, 46*]. Madariaga [*32*] summarized some interesting analytic scaling relationships related with a single corner ω^2 spectrum. For example, he noted that the ratio of total seismic radiated energy (E_R) and seismic moment (M_0) can be represented as

$$E_R/M_0 \sim C_r M_0 f_c^3/(\mu\beta^3) \qquad (12)$$

C_r is a constant about 2, f_c, μ, β denote the corner frequency, rigidity and shear wave speed, respectively. Hence, for a given earthquake, the E_R/M_0 ratio or more often quoted apparent stress σ_a ($\sigma_a = \mu\, E_R/M_0$) scales with f_c^3—close to the relation between PGA and f_c. It motivates us to evaluate the total radiated seismic energy of different solutions. For the purpose of simplification, all of discussion presented below is for a symmetric circular rupture with a constant rupture velocity of 0.9β. Using the Brune type relation $f_c = 0.49\beta(\Delta\sigma_B/M_0)^{1/3}$ with $\Delta\sigma_B$=4.64 MPa [*28*] and μ=3.3x10^4 MPa, the predicted E_R/M_0 ratio is 3.3x10^{-5}, independent of magnitude. σ_a is 1.1 MPa. By taking bandwidth limitations of seismic recordings into consideration Ide and Beroza [*47*] corrected three published datasets over magnitude range

from 0.5 to 9; they found a nearly constant ratio of radiated energy to seismic moment, $3x10^{-5}$, or 1.0 MPa for apparent stress. Convers and Newman [*48*] recently studied 342 Mw>6.7 earthquakes from 1990 to 2010 and reported a nearly identical average E_R/M_0 ratio of $2.6x10^{-5}$ with a factor of 2.3 uncertainty. Hence, the scaling relation of f_c inferred from [*28*] is in excellent agreement with the current knowledge about seismic radiated energy. For Brune's model [*3*] the ratio of apparent stress and static stress drop ($\sigma_a/\Delta\sigma$) is also independent of magnitude. It is 0.233 for a rupture velocity of 0.9β, Madariaga [*41*]. However, if we instead use the aforementioned relationship for corner frequency based on the results of [*11*], $\log(f_c^s) = 2.164 - 0.5M$ (Section 3.2), $E_R/M_0 = 0.49x10^{-5}$; 6.8 times smaller than Ide and Beroza [*47*] or Convers and Newman [*48*]; σ_a is 0.16 MPa. $\sigma_a/\Delta\sigma$ is less than 0.05 if we use $\Delta\sigma_M$ as $\Delta\sigma$.

Both models [*3*] and [*41*] are currently used for interpreting seismic data. For an earthquake that is modeled with a dynamic circular crack with constant rupture velocity, the model [*41*] aims to provide a better link between its mean corner frequency and source radius than the model in [*3*]. However, the mean corner frequency referred to in [*41*] is the spherical mean of individual corner frequency measures at different take-of angles; the corner frequency varies by a factor of 2-3 [*41, 49*]. Radiated seismic energy is proportional to f_c^3. The cube of the spherical mean of f_c is not same as the spherical mean of f_c^3. The predicted radiated energy, as well as apparent stress σ_a, using [*41*] are much lower than the values found in dynamic calculations [*49, 50*]. Results from [*49, 50*] show that when ratio of rupture velocity and shear wave speed is 0.9, $\sigma_a/\Delta\sigma$ is 0.238 (inferred from Table 1, [*50*]), nearly identical to the prediction 0.233 in Brune's model [*3*]. Hence, for a given earthquake, the Madariaga model [*41*] is better in estimating its rupture area and average static stress drop, and the Brune model might be better predicting its high frequency radiation and total radiated seismic energy. Neither can explain both the static stress drop and radiated energy simultaneously.

We have numerically calculated E_R/M_0 and σ_a for our preferred double-corner source spectrum defined by equation (10) for earthquakes $5.3 \leq M \leq 7.7$. We obtain $E_R/M_0 = 2.0x10^{-5}$ and σ_a=0.68 MPa, independent of magnitude. Given the uncertainty in estimating seismic radiated energy, the agreement with [*47*] and [*48*] is excellent.

It is worthwhile to point out that if we use $f_c^p/f_c^s = 1$ in the above discussion, E_R/M_0 and $\Delta\sigma_a$ will be 2.0x10^{-5} and 0.68 MPa, respectively. It provides an alternative way to explain the above discrepancy. For large earthquakes, the rupture is more appropriately modeled as slip pulse, which will produce a double corner spectrum [*1*] rather than an expanding crack. The corner frequency inferred from the P wave is same as that inferred from the S wave.

4. Conclusions

Following our paper [*33*] for earthquakes $3.3 \leq M \leq 5.3$, we have derived a double-corner source spectrum for S waves for $M \geq 5.3$. Using random vibration theory, we show that this spectrum produces PGA and PGV that matches the data from NGA West-2 [*26*]. The lower corner f_{c1} is within 18% of the corner one would observe from the global CMT catalog [*43*], i.e., it's inverse $1/\pi f_{c1}$ corresponds to the duration of earthquakes found worldwide. The acceleration spectrum has a f^1 slope between the lower and higher corner f_{c2}. Above f_{c2} the acceleration spectrum is flat, ~ f^0; the level of the spectrum for $f > f_{c2}$ is consistent with the stress parameter that is the source of PGA and PGV. We have shown that the ratio of radiated

energy to seismic moment and apparent stress are independent of magnitude and are approximately the same as that found for global earthquakes in the same magnitude range [*47*], [*48*].

5. Acknowledgments and Data

We used data in the Excel file "NGA_West2_Flatfile_RotD50_d005_public_version" available from the Pacific Earthquake Engineering Research Center at the website http://peer.berkeley.edu/ngawest2/databases/. This study is supported by NSF grant EAR-1215769 and by grants from the Southern California Earthquake Center (SCEC)—funded by NSF cooperative agreement EAR-0109624 and USGS cooperative agreement 02HQAG0008. We received support from UCSB matching grants to SCEC. We appreciate the collection, archiving, and quality control of data under NGA-West2. We thank all organizations that have invested in deploying and maintaining high-quality seismic sensors that record earthquakes for a wide range of magnitudes. All calculations are done with open-source Julia language and figures are created with GMT.

6. References

1. A. A. Gusev, High-frequency radiation from an earthquake fault: A review and a hypothesis of fractal fupture front geometry. *Pure Appl Geophys* **170**, 65-93 (2013).
2. N. Haskell, Total energy and energy spectral density of elastic wave radiation from propagating faults, B. Seismol. Soc. Am. **56**, 1811 –1842 (1964).
3. J. N. Brune, Tectonic stress and spectra of seismic shear waves from earthquakes. *J Geophys Res* **75**, 4997-5009 (1970).
4. S. Das, B. V. Kostrov, Breaking of a single asperity - rupture process and seismic radiation. *J Geophys Res* **88**, 4277-4288 (1983).
5. A. A. Gusev, Descriptive statistical-model of earthquake source radiation and its application to an estimation of short-period strong motion. *Geophys J Roy Astr S* **74**, 787-808 (1983).
6. A. S. Papageorgiou, K. Aki, Scaling law of far-field spectra based on observed parameters of the specific barrier model. *Pure Appl Geophys* **123**, 353-374 (1985).
7. J. Boatwright, The seismic radiation from composite models of faulting. *B Seismol Soc Am* **78**, 489-508 (1988).
8. T. H. Heaton, Evidence for and implications of self-healing pulses of slip in earthquake rupture. *Phys Earth Planet In* **64**, 1-20 (1990).
9. K. Aki, Asperities, barriers, characteristic earthquakes and strong motion prediction, *J Geophys Res* **89,** 5867-5872 (1984)
10. H. Kanamori, D. L. Anderson, Theoretical basis of some empirical relations in seismology. *B Seismol Soc Am* **65**, 1073-1095 (1975).
11. B. P. Allmann, P. M. Shearer, Global variations of stress drop for moderate to large earthquakes. *J Geophys Res-Sol Ea* **114**, (2009).
12. S. Hartzell, J. N. Brune, Horse Canyon earthquake of August 2, 1975 -2- stage stress-release process in a strike-slip earthquake. *B Seismol Soc Am* **69**, 1161-1173 (1979).
13. G. L. Choy, J. Boatwright, The rupture characteristics of 2 deep earthquakes inferred from broad-band Gdsn data. *B Seismol Soc Am* **71**, 691-711 (1981).
14. E. Faccioli, A study of strong motions from Italy and Yugoslavia in terms of gross source properties, in *Earthquake Source Mechanics*, *AGU Geophysical Monograph* **37**, Eds., S. Das, J. Boatwright and C. Scholz, 297-309 (1986).

15. N. A. Haskell, Total energy and energy spectral density of eastic wave radiation from propagating faults .2. A statistical source model. *B Seismol Soc Am* **56**, 125-& (1966).
16. G. M. Atkinson, Earthquake source spectra in Eastern North-America. *B Seismol Soc Am* **83**, 1778-1798 (1993).
17. K. Aki, Scaling law of seismic spectrum. *J Geophys Res* **72**, 1217-& (1967).
18. D. Garcia, S. K. Singh, M. Herraiz, J. F. Pacheco, M. Ordaz, Inslab earthquakes of Central Mexico: Q, source spectra, and stress drop. *B Seismol Soc Am* **94**, 789-802 (2004).
19. G. M. Atkinson, T. C. Hanks, A high-frequency magnitude scale. *B Seismol Soc Am* **85**, 825-833 (1995).
20. G. M. Atkinson, I. Beresnev, Don't call it stress drop. *Seismological Research Letters* **68**, 3-4 (1998).
21. D. M. Boore, C. Di Alessandro, N. A. Abrahamson, A generalization of the double-corner-frequency source spectral model and its use in the SCEC BBP validation exercise. *B Seismol Soc Am* **104**, 2387-2398 (2014).
22. C. A. Goulet, N. A. Abrahamson, P. G. Somerville, K. E. Wooddell, The SCEC Broadband platform validation exercise: methodology for code validation in the context of seismic-hazard analyses. *Seismological Research Letters* **86**, 17-26 (2015).
23. D. M. Boore, Simulation of ground motion using the stochastic method. *Pure Appl Geophys* **160**, 635-676 (2003).
24. A. S. Baltay, T. C. Hanks, Understanding the magnitude dependence of PGA and PGV in NGA-West 2 data. *B Seismol Soc Am* **104**, 2851-2865 (2014).
25. T. C. Hanks, R. K. Mcguire, The character of high-frequency strong ground motion. *B Seismol Soc Am* **71**, 2071-2095 (1981).
26. Y. Bozorgnia, N. A. Abrahamson, L. Al Atik, T. D. Ancheta, G. M. Atkinson, J. W. Baker, A. Baltay, D. M. Boore, K. W. Campbell, B. S. J. Chiou, R. Darragh, S. Day, J. Donahue, R. W. Graves, N. Gregor, T. Hanks, I. M. Idriss, R. Kamai, T. Kishida, A. Kottke, S. A. Mahin, S. Rezaeian, B. Rowshandel, E. Seyhan, S. Shahi, T. Shantz, W. Silva, P. Spudich, J. P. Stewart, J. Watson-Lamprey, K. Wooddell, R. Youngs, NGA-West2 research project. *Earthq Spectra* **30**, 973-987 (2014).
27. D. M. Boore, Stochastic simulation of high-frequency ground motions based on seismological models of the radiated spectra. *B Seismol Soc Am* **73**, 1865-1894 (1983).
28. J. G. Anderson, S. E. Hough, A model for the shape of the Fourier amplitude spectrum of acceleration at high-frequencies. *B Seismol Soc Am* **74**, 1969-1993 (1984).
29. J. E. Luco, On strong ground motion estimates based on models of the radiated spectrum. *B Seismol Soc Am* **75**, 641-649 (1985).
30. D. M. Boore, W. B. Joyner, Site amplifications for generic rock sites. *B Seismol Soc Am* **87**, 327-341 (1997).
31. T. C. Hanks, H. Kanamori, Moment magnitude scale. *J Geophys Res* **84**, 2348-2350 (1979).
32. R. Madariaga, Earthquake scaling laws. 364-383 (2011).
33. R. J. Archuleta, C. Ji, Moment rate scaling for earthquakes 3.3M5.3 with implications for stress drop. *Geophys Res Lett* **43**, 12004-12011 (2016).
34. M. A. Meier, T. Heaton, J. Clinton, Evidence for universal earthquake rupture initiation behavior. *Geophys Res Lett* **43**, 7991-7996 (2016).
35. W. L. Ellsworth, G. C. Beroza, Seismic evidence for an earthquake nucleation phase. *Science* **268**, 851-855 (1995).
36. J. Boatwright, Spectral theory for circular seismic sources - simple estimates of source dimension, dynamic stress drop, and radiated seismic energy. *B Seismol Soc Am* **70**, 1-27 (1980).
37. R. A. W. Haddon, Earthquake source spectra in eastern North America. *B Seismol Soc Am*

86, 1300-1313 (1996).

38. R. K. Mcguire, T. C. Hanks, RMS accelerations and spectral amplitudes of strong ground motion during the San-Fernando, California earthquake. *B Seismol Soc Am* **70**, 1907-1919 (1980).
39. D. E. Cartwright, M. S. Longuethiggins, The statistical distribution of the maxima of a random function. *Proc R Soc Lon Ser-A* **237**, 212-232 (1956).
40. G. M. Atkinson, D. M. Boore, Ground-motion relations for eastern North America. *B Seismol Soc Am* **85**, 17-30 (1995).
41. R. Madariaga, Dynamics of an expanding circular fault. *B Seismol Soc Am* **66**, 639-666 (1976).
42. G. Ekstrom, A. M. Dziewonski, N. N. Maternovskaya, M. Nettles, Global seismicity of 2003: centroid-moment-tensor solutions for 1087 earthquakes. *Phys Earth Planet In* **148**, 327-351 (2005).
43. G. Ekstrom, E. R. Engdahl, Earthquake source parameters and stress-distribution in the Adak Island region of the Central Aleutian Islands, Alaska. *J Geophys Res-Solid* **94**, 15499-15519 (1989).
44. H. Kanamori, L. Rivera, Static and dynamic scaling relations for earthquakes and their implications for rupture speed and stress drop. *B Seismol Soc Am* **94**, 314-319 (2004).
45. F. Cotton, R. Archuleta, M. Causse, What is sigma of the stress drop? *Seismological Research Letters* **84**, 42-48 (2013).
46. A. S. Baltay, T. C. Hanks, G. C. Beroza, Stable stress-drop measurements and their variability: implications for ground-motion prediction. *B Seismol Soc Am* **103**, 211-222 (2013).
47. S. Ide, G. C. Beroza, Does apparent stress vary with earthquake size? *Geophys Res Lett* **28**, 3349-3352 (2001).
48. J. A. Convers, A. V. Newman, Global evaluation of large earthquake energy from 1997 through mid-2010. *J Geophys Res-Sol Ea* **116**, (2011).
49. Y. Kaneko, P. M. Shearer, Seismic source spectra and estimated stress drop derived from cohesive-zone models of circular subshear rupture. *Geophys J Int* **197**, 1002-1015 (2014).
50. Y. Kaneko, P. M. Shearer, Variability of seismic source spectra, estimated stress drop, and radiated energy, derived fromcohesive-zonemodels of symmetrical and asymmetrical circular and elliptical ruptures. *J Geophys Res-Sol Ea* **120**, 1053-1079 (2015).